Materials & Design, Volume 115, 5 February 2017, pp. 26–36
DOI:10.1016/j.matdes.2016.11.025

Influence of Z-pin embedded length on the interlaminar traction response of multi-directional composite laminates

Mehdi Yasaee[1*], Lawrence Bigg[2], Galal Mohamed[2], Stephen R. Hallett[2]

[1] *School of Aerospace, Transport and Manufacturing, University of Cranfield, Cranfield, MK43 0AL, UK*

[2] *Advanced Composites Centre for Innovation and Science (ACCIS), University of Bristol, Queen's Building, University Walk, Bristol, BS8 1TR, UK*

* *m.yasaee@cranfield.ac.uk +44(0)1234 75 4384*

Abstract

The work in this paper investigated the performance of composites through-thickness reinforcing Z-pins as a function of their embedded length in pre-preg laminates. Single Z-pins were inserted into multidirectional carbon fibre laminates with increasing thicknesses, corresponding to embedded lengths from 1mm to 10mm and tested through a range of mixed mode displacement ratios to investigate their interlaminar bridging traction response. Detailed analysis of the tests revealed a non-linear tangential friction response and its strong dependence on the embedded length of the Z-pin. Using a new power law empirical relationship for the tangential friction force per unit length, a modified Z-pin bridging traction analytical model was proposed, giving good predictions of the full mixed mode bridging mechanics of a CFRP Z-pin in a multidirectional composite laminate of varying thickness. Several characteristics of the model are discussed and their influence on the predicting the Z-pin bridging energy response have been analysed.

Keywords

Structural composites; Z-pins; Delamination; Fracture toughness; Analytical model

1 Introduction

The pursuit of improving the thickness direction integrity of fibre reinforced plastic (FRP) composite materials has produced many technologies that can provide significant improvements with the addition of through thickness reinforcement (TTR) elements [1]. For pre-impregnated FRP composite laminates the most viable technology is Z-pinning, which is a process of inserting small, stiff, FRP or metallic pins in the thickness direction of an uncured composite laminate. These pins are then capable of providing substantial resistance to inter-laminar crack propagation or delamination in the FRP laminate, effectively increasing their apparent fracture toughness [2,3]. However, these pins are a secondary component in the material, meaning their contribution to the traction loads in a delaminated composite depends strongly on their respective materials, geometry and their physical interaction with the host material [4,5]. These responses can thus be uncoupled from the full delamination response, by treating the cohesive traction of a composite and the bridging traction introduced with addition of Z-pins separately. In this way, the influence of the Z-pins' bridging behaviour can be analysed with greater detail [4,6,7], which can subsequently produce bridging traction models for prediction of full delamination resistance behaviour of FRP composites with arrays of Z-pins [8–10].

The geometry of the pins plays a major role in determining their performance in improving the composite laminates' through thickness integrity. The traction response of a Z-pin in a delaminated composite material when loaded in mode I is influenced by four parameters; the pin and the bond strength with the matrix, the frictional contact between the pin and the host material, the elastic modulus and the tensile strength of the pin if pull-out does not occur and pin fracture [6]. The bond strength and the subsequent frictional pull-out is a function of the pin embedded length in the material and its surface condition such as roughness [4,7,11,12]. The residual stresses in the host and the pin material due to manufacturing conditions also play a significant role in its response, which is particularly evident between composite laminates with unidirectional (UD) or multi-directional laminates [4,13]. For mode II delamination, the traction response of a Z-pin is dominated by the pin material's transverse shear strength and its local bond integrity in the vicinity of the crack surfaces [4,6,9,14].

In most commercial uses of Z-pin technology the pin diameter is nominally 0.28mm, made from Carbon FRP (CFRP). However, the embedded length of the Z-pins in the laminate will vary, depending on the thickness of the component being reinforced. The apparent embedded length will also vary when multiple delamination are formed [15] or in situations when the Z-pins have different penetration depths [16]. Despite its important influence on the traction response, the Z-pin embedded length has been the subject of only a very limited number of studies. Mouritz *et. al.* [7] investigated an array of Z-pins in UD laminates tested in pure mode I. They showed that an increase in embedded length from 0.6mm to 4mm increased the number of pins fracturing rather than pulling out. For 4mm embedded length 100% of the pins appeared to completely fracture. In their investigation, the misalignments inherent in the pins were used to analyse the data up to a small range of mixed mode ratios, but this was not sufficient to provide the full mode mixity trend for different embedded lengths of Z-pins. An investigation by Pegorin *et. al.* [16] was concerned with the relationship between Z-pin embedded length and the mode I and mode II fracture toughness and fatigue resistance of standard UD FRP composite test coupons. These tests showed that an increase in embedded length provide a higher resistance to mode I delamination growth but lower resistance to mode II delamination. These studies on embedded length behaviour have however only considered UD laminates. No literature exists measuring the influence of embedded length on the traction response of Z-pinned laminates tested across the full range of mode I, mixed mode I/II and mode II loading in multidirectional laminates.

Modelling Z-pinned reinforcements in FRP composites have been the subject of numerous studies [6,8,9,17–25]. In most cases, researchers have implemented a Z-pinned interface bridging law in a Finite Element (FE) framework to predict behaviour of standard fracture toughness test specimens [8,18,23] or structural T-joints [20,26]. Only two investigations demonstrated a mixed-mode Z-pin traction bridging law [8,24], however these studies have been limited to a single thickness of composite laminate.

In this paper experimental testing has been carried out to characterise the behaviour of Z-pins with embedded lengths of 1mm, 5mm, and 10mm when tested at 0°, 30°, 60° and 90° mixed mode angles, corresponding to pure mode I, mixed mode I/II (38% and 49%) and pure mode II loading. The

measured response of the Z-pins is compared with earlier experiments in [4] and an analytical micro-mechanical model of individual Z-pins subjected to mixed-mode loading developed in [24]. In this model Z-pins are described as a Euler–Bernoulli beams undergoing small but finite rotations upon elastic deformation. New modifications to this model are proposed in this paper and fitted against the new data to generate a comprehensive traction response map, for a range of Z-pin embedded length, which can be implemented in a numerical FE framework [25].

2 Specimen Preparation

Composite panels made from IM7/8552 pre-preg material (Hexcel, UK) were produced with a Quasi Isotropic (QI) stacking sequence. To unambiguously measure only the Z-pin bridging forces, it is essential to remove the effect of the laminate interface by introducing an artificial delamination. Four panel thicknesses were manufactured; 2mm with $[(0/45/90/-45)_S$ // $(90/-45/0/45)_S]$, 10mm with $[(0/45/90/-45)_{5S}$ // $(90/-45/0/45)_{5S}]$ and 20mm with $[(0/45/90/-45)_{10S}$ // $(90/-45/0/45)_{10S}]$ sequence. The symbol // indicates the location of the mid-plane where a 20μm release film insert was embedded. The stack orientation on the mid-plane was always 0/90, ensuring the two laminate halves do not intermingle during consolidation. This is particularly important for tests with a mode II loading component as intermingled layers will effectively interlock and thus produce incorrect larger traction forces.

For each specimen, a 0.28mm T300 carbon/BMI pin was inserted manually into the laminate ensuring full insertion was achieved with no damage or splitting. The final cured specimen was machined from the larger plates to the final geometry as shown in Figure 1. For all the specimens, a small length of pin protruded from the surface of the laminated after the cure process. These pultruded ends were sanded down in order for the specimen to sit flush in the test fixtures. Readers must note that results of these experiments only apply to full thickness penetrated pins.

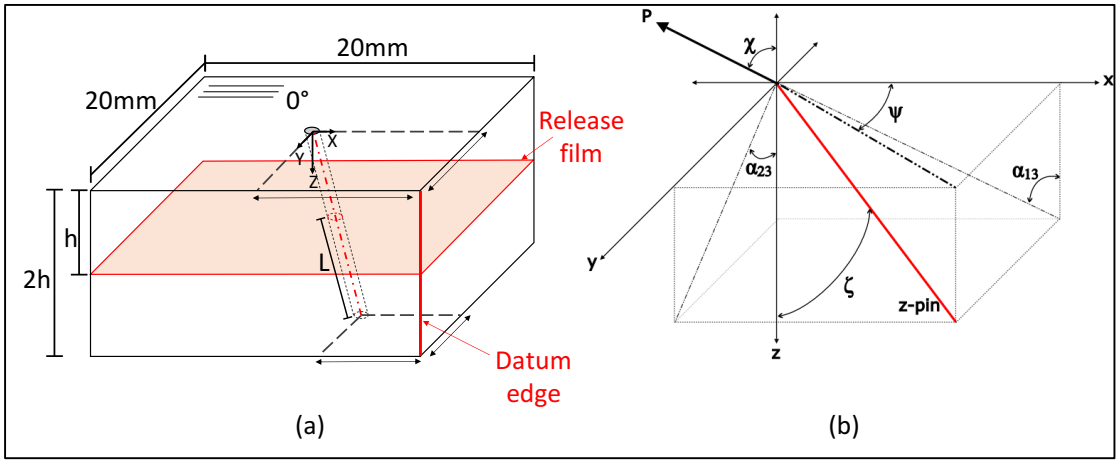

Figure 1 (a) Geometry of the test specimens highlighting the specimen thickness, 2h, the embedded Z-pin length h and the datum edge for Z-pin misalignment angle measurement (b) Coordinate axis and angle definitions

The individual pin-misalignment angles were measured after each specimen was machined to its final geometry. The X and Y distance of the top and bottom of the pin was measured from the datum edge, Figure 1a. Using these measurements, the in-plane misalignment angles $\alpha 13$ and $\alpha 23$ and subsequently the relative offset angle from the vertical (z-axis), ζ, and the deviation from the 0° fibre direction (x-axis), ψ were calculated using the coordinate axis convention (Figure 1b) and the following relationships [4]:

$$\tan\zeta = \sqrt{\tan^2\alpha_{13} + \tan^2\alpha_{23}} \tag{1}$$

$$\tan\psi = \frac{\tan\alpha_{23}}{\tan\alpha_{13}} \tag{2}$$

3 Test Procedure

All tests were conducted on an Instron 1341 servo hydraulic test rig, using a 1kN load cell following the procedure given in [4]. Each specimen was attached to its respective test fixture using Loctite© 'Super Glue'. Before the glue sets the specimen was gently loaded in compression to no more than -50N so as to achieve the necessary high strength bond. Each specimen was marked with six tracking dots, three on each half of the specimen, to directly measure the displacement using a non-contact video extensometer (Imetrum Ltd). This ensured that the displacement data of the specimen was free from any compliance ambiguity that may results from the glue and the test fixtures.

All specimens were loaded at a displacement rate of 0.5mm/min. Mixed mode loading was introduced into the specimens by fixing their Y-axis orientation, χ (Figure 1b) at 0°, 30°, 60° and 90°. The total force acting on the pin (P) can be resolved in terms of the pin axis as:

$$P = \begin{bmatrix} N \\ X_x \\ X_y \end{bmatrix} = \begin{bmatrix} \sin\zeta\cos\psi & \sin\zeta\sin\psi & \cos\zeta \\ \cos\zeta\cos\psi & \cos\zeta\sin\psi & -\sin\zeta \\ -\sin\psi & \cos\psi & 0 \end{bmatrix} \begin{bmatrix} P\sin\chi \\ 0 \\ P\cos\chi \end{bmatrix} \quad (3)$$

Where N is the axial load and X_x and X_y are the shear loads acting on the pin. Introducing the load mixed mode ratio (ϕ) as the ratio of the shear loads (X) to the total load (P):

$$\phi = \frac{X}{P} = \frac{X}{\sqrt{N^2 + X^2}} = \sqrt{\frac{X_x^2 + X_y^2}{N^2 + X_x^2 + X_y^2}} \quad (4)$$

The precise mixed mode angle, ω, as seen by the pin, including the effect of its misalignment, can then be calculated for each specimen using:

$$\omega = \tan^{-1}\left(\frac{\phi}{\sqrt{1-\phi^2}}\right) \quad (5)$$

For a perfectly orthogonal pin (ζ, ψ=0°) the orientation, χ is directly equal to the mixed mode angle, ω. The nominal mixed mode angles tested in this investigation correspond to loading mixed mode ratios of Mode I, 38% and 49% Mixed Mode I/II and Mode II, respectively. The misalignment of each individual pin inside the specimens was measured directly and the mixed mode angle, ω corrected accordingly, which resulted in some variation in the exact mixed mode ratio experienced by each pin in each series of tests at a nominal angle. For clarity each of the mixed mode tests will be labelled with the nominal mixed mode angles given above, but the actual mixed mode angles will be used in the plotting of the data and calculations.

The three specimen nominal thicknesses tested were, 2mm, 10mm and 20mm. The release film simulating the delamination was placed on the mid plane, therefore the effective embedded length, L^{-} of the Z-pin is nominally equivalent to the sample half thickness, h; being 1mm, 5mm and 10mm respectively. With the exception of cases where large scatter was found in the load-displacement data, a minimum of 3 specimens were tested per configuration.

4 Results

4.1 Traction Response

The traction load, P and displacement, δ results for all the mixed mode tests are given in Figure 2.

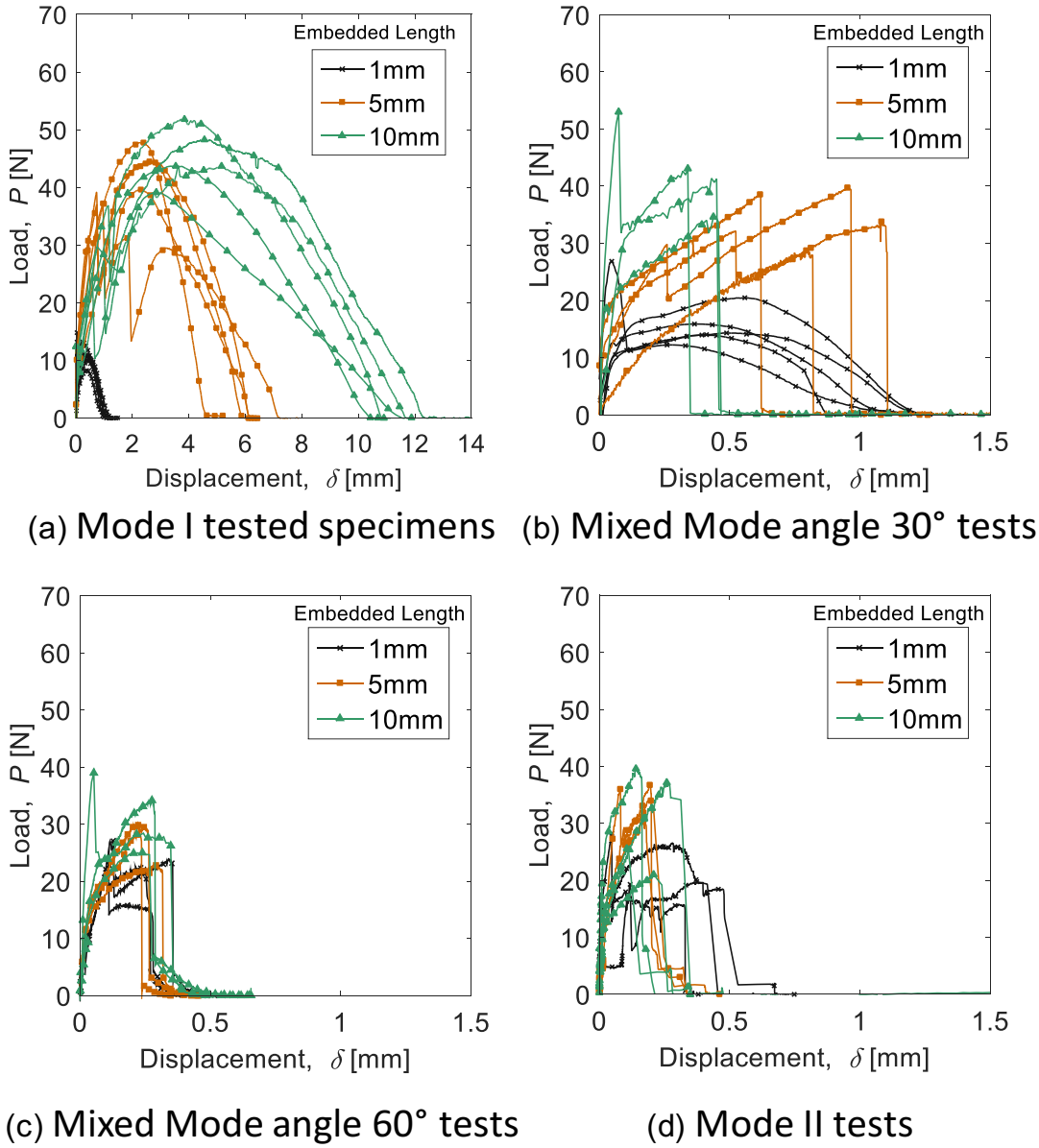

Figure 2 Load, *P* vs. Displacement, *δ* plots for all mixed mode tests

The load trends in the Mode I tests (Figure 2a) follow the expected two stage response of pin pull-out [2,7,27]. In the first stage, the pin is loaded elastically until the pin/matrix bond limit is reached and the pin debonds from the surrounding matrix. This is seen as a sudden load drop. Since the Z-pin

embedded length above and below the mid-plane is nominally equal, the segment of the pin that debonds first may be in either half of the laminate. This stage is followed by the pull-out phase when the pin slides out of the specimen and the traction load is dominated by the interface friction between the pin and the matrix. Ideally, it is expected for the pull-out length to be equivalent to the embedded length, L^{-}. However, the specimens average pull-out length for specimens of 1mm, 5mm and 10mm was measured to be longer, at 1.09±0.11mm, 6.07±0.73mm and 11.30±0.74mm respectively. This is caused by the combination of simultaneous pull-out of the pin from both laminate halves as well as the misalignment of the pins which effectively increased the average embedded lengths. For clarity, the average embedded lengths will be referred to by their nominal 1mm, 5mm and 10mm lengths, however for any calculations of individual samples the correct embedded length was used.

Using scanning electron microscope (SEM) imaging shown in Figure 3, the representative failures observed across the mixed mode tests are shown. For mode I tests for all embedded length tests, specimens exhibited full pull-out, with no evidence of splitting or noticeable damage, Figure 3a.

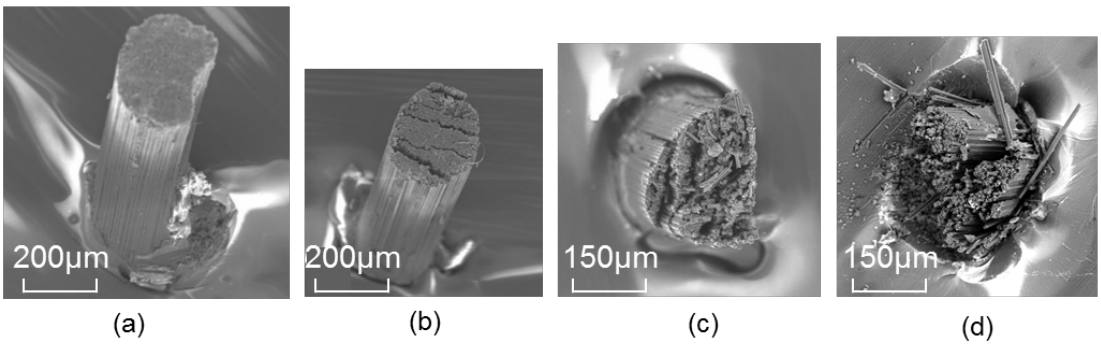

Figure 3 SEM images showing typical failure profiles (a) Full pull-out with no internal damage, (b) Full pull-out with internal splitting, (c) Partial pull-out with internal splitting before fracture, (d) Shear dominated fracture with some evidence of internal splitting and partial pull-out

For the mixed mode angle of 30° there was some variability in the failure mode with embedded length, as can be observed from the P-δ plot in Figure 2b. The 1mm embedded length specimens, show complete pull out with a very similar profile to that of the Mode I tests, however some internal splitting were observed during this process, Figure 3b. As expected, with increase in embedded length the pin/matrix interface friction force becomes higher and is enhanced with increasing mixed mode angles. For 5mm and 10mm embedded lengths, this enhanced friction, increases the load experienced

by the pin until its failure limit is reached during pull-out stage. However, the frictional enhancement of the 5mm embedded length is less than those in the 10mm samples, allowing the 5mm samples to partially pull-out, causing internal splitting, which reduces the residual stiffness of the Z-pin and results in longer displacement to failure.

For mixed mode angle of 60° tests all three embedded length samples resulted in pin fracture (*P*-δ plot in Figure 2c). In comparison with the 30° mixed mode tests there is a minor decrease in the maximum pin failure load. The specimens all exhibited fracture with only partial pull-out, similar to Figure 3c with comparable interface stiffness of the traction response.

The pure mode II tests exhibit pin failure for all three embedded length specimens (*P*-δ plot in Figure 2d). Only the 1mm embedded length specimens showed a minor increase in failure displacement. This discrepancy is associated with the initial pin misalignments which either increase or decrease the pin mixed mode angle relative to the loading direction, resulting in, with the nap or against the nap loading [4,28]. The fracture profile for the 1mm embedded lengths showed split ends and minor pull-out lengths similar to Figure 3c , whereas the 5mm and 10mm embedded length samples showed very little pull-out before shear dominated fracture as shown in Figure 3d.

4.2 Bridging Energy

For each mixed mode angle, ω the total Z-pin traction energy absorbed, Ω was calculated by integrating the *P*-δ curves from the origin until the maximum displacement, δ_{max} when the specimen either completed its pull-out process or fractured, thus:

$$\Omega(\omega) = \int_0^{\delta_{max}} P \, d\delta \tag{6}$$

The plots of energy absorbed against the mixed mode angle, ω are given in Figure 4. As expected there exists a transition region (red patch) where the pins are on the boundary between either pull-out or fracture. This region is bounded by the maximum and minimum mixed mode angle at which a pin exhibited complete pull-out or fracture during the testing, respectively. Yasaee *et. al.* [4] showed this transition region to be 11°-18° in UD laminates as compared to 33°-37° in QI laminates for 4mm embedded length Z-pins. The test results here highlight the influence of embedded length on this

transition region. For pin embedded length of 1mm the transition region was calculated to be between 28°-51°, for 5mm to be 9.1°-25.4° and for 10mm to be 5.5°-26.9° as shown in Figure 4a-c. There is a clear trend for the transition region to decrease with increase in embedded length of the Z-pins, however the resolution of the mixed mode angles tested here does not provide enough data points to capture a narrow transition region. To capture a clear and narrow transition region per embedded length, more samples need to be tested within those transition region bands.

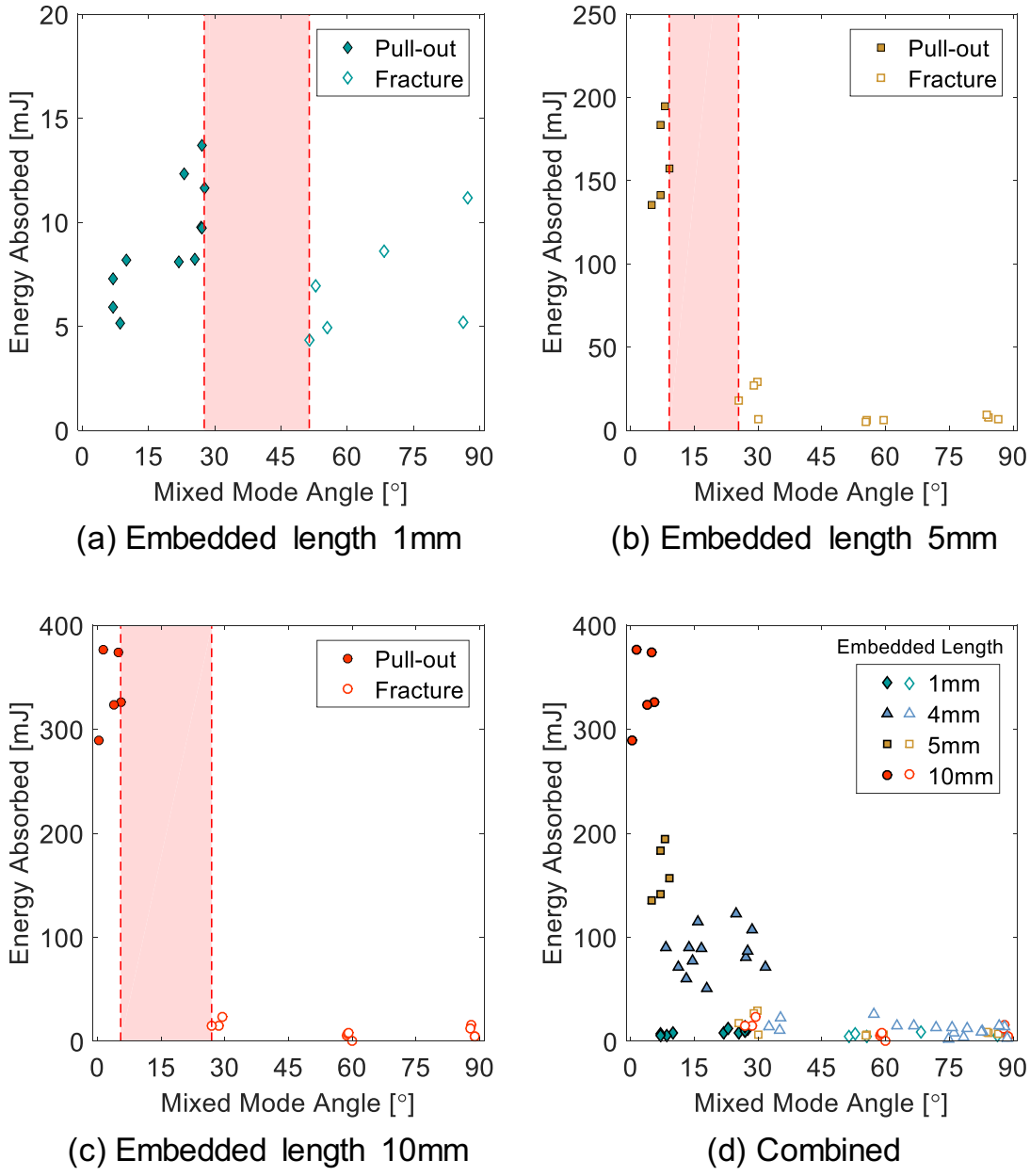

Figure 4 Traction work done (Energy absorbed)-mixed mode angle plot for embedded lengths (a) 1mm, (b) 5mm, (c) 10mm and (d) combined plots including data from 4mm embedded length tests [4]**. (Solid symbols are full pull-out; white filled symbols are fractured)**

As expected, the total pull-out energy increases with increasing embedded lengths. For each embedded length, there is an increase in absorped energy with increasing mode II component of the load, for those specimens that experienced pull-out. However, large scatter in the data does not provide a reliable measurement of the slope. The mode II dominated response for all embedded lengths produced comparable energies to fracture.

These experimental tests provide new understanding on the friction response of the Z-pins, which can be used to modify the analytical Z-pin traction model, discussed in section 5, for prediction of the transition regions and the increase in the pull-out energy with mixed mode angle.

4.3 Effective shear strength

With increase in mixed mode ratio the Z-pins traction response transitions from complete pull-out to a combination of pull-out and fracture. For the test conditions that resulted in fracture of the Z-pins, the failure mode is a mixture of tensile and shear fracture with internal splitting. The analysis of Z-pin failure mode changes with increased mode mixity has been the subject of numerical investigations, which detailed the micro-mechanisms of the failure process [9,27]. These studies demonstrated the influence of Z-pin tensile and shear strength, as well as longitudinal splitting, on the bridging traction response and were successful in predicting the full traction response of an individual Z-pin for a range of mixed mode tests. However, such a high fidelity modelling approach is not practical for predicting Z-pin failures in large scale structures. Given that the presence of splitting becomes evident with the inclusion of a shear component in the load, it is possible to simplify the complex failure modes of the Z-pin into an effective property for the Z-pin shear strength, τ_f. By considering a linear failure criterion, a Z-pin is deemed to have failed when its failure index reaches 1:

$$\frac{\sigma_z}{\sigma_{zf}} + \frac{\tau}{\tau_f} = 1 \qquad (7)$$

Where σ_z and σ_f are the axial stress and strength of the Z-pin respectively and τ is the average shear stress in the cross-section of the Z-pin. σ_z and τ are calculated from the axial and shear loads over the cross sectional area of the Z-pin, A. By inserting the mixed mode relationship defined in equations (4)

and (5) into the linear failure criterion in equation (7), the relationship between the fracture load, P_f and the mixed mode angle, ω can be rearranged to be:

$$P_f = \frac{A\sigma_{zf}\tau_f\sqrt{\tan^2\omega + 1}}{\sigma_{zf} + \tau_f \tan\omega} \tag{8}$$

From the experimental data, the fracture load, P_f of all the specimens which did not exhibit pull-out is plotted against the mixed mode angle, ω in Figure 5.

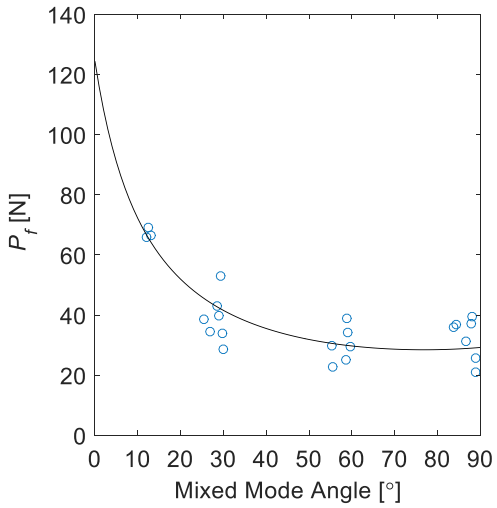

Figure 5 Pin failure load against increasing mixed mode angle. Solid line is the linear failure criterion from equation (23) for σ_{zf} of 2026MPa and τ_{xf} of 485MPa

By setting the Z-pin tensile strength, σ_{zf} to be 2026MPa [29], a least square quadratic curve fit of equation (8) to the data in Figure 5 yields an Z-pin effective shear strength, τ_f of 485MPa. This value is much higher than a typical Z-pin shear strength, which is on the order of 100MPa. This indicates that extra failure mechanisms beyond simple shearing of the pin such as pin splitting and pull-out are contributing to this effective shear strength. Therefore, with the utilisation of this homogenised failure criterion, the failure load of the Z-pins can be predicted without the need for complex models predicting Z-pin splitting behaviour.

5 Bridging Traction Model

The bridging traction of a Z-pin on a delaminated surface can be predicted using a semi-analytical model developed by Allegri *et. al.* [24]. Consider a Z-pin of total length L, embedded into a composite laminate as shown in Figure 6.

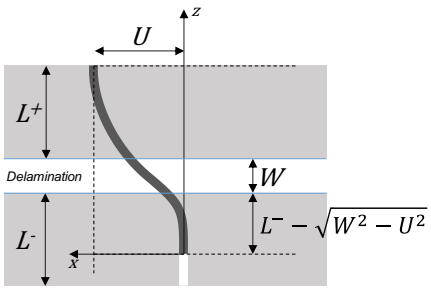

Figure 6 Assumed bridging kinematics of the Z-pin showing opening and sliding mode

The mixed-mode delamination that splits the two halves of the laminate intersects the Z-pin at a specific length along its axis. The Z-pin then contributes a bridging force on the delaminated surfaces to counteract the opening/sliding displacements. The ratio of the embedded length to the total length can be defined as:

$$\alpha = \frac{L^-}{L^- + L^+} = \frac{L^-}{L} \tag{9}$$

For symmetric intersection of the Z-pin with respect to the delamination plane, α=1/2. The segment of the Z-pin that pulls-out is assumed to be the lower half, with embedded length, *L,* which progressively shortens with increase in total displacement, δ. Any sliding displacement, U will increase the contribution of the shear forces of the Z-pin. The mixed mode ratio, ϕ is equivalent to the ratio of the sliding displacement to the total displacement:

$$\phi = \frac{U}{\sqrt{U^2 + W^2}} = \frac{U}{\delta} \tag{10}$$

The Z-pin shown in Figure 6 is modelled as a Euler-Bernoulli beam subjected to a small but finite rotation. The original bridging traction model and calibrated parameters presented in [24] is plotted in Figure 7, for increasing Z-pin embedded lengths, along with the experimental data.

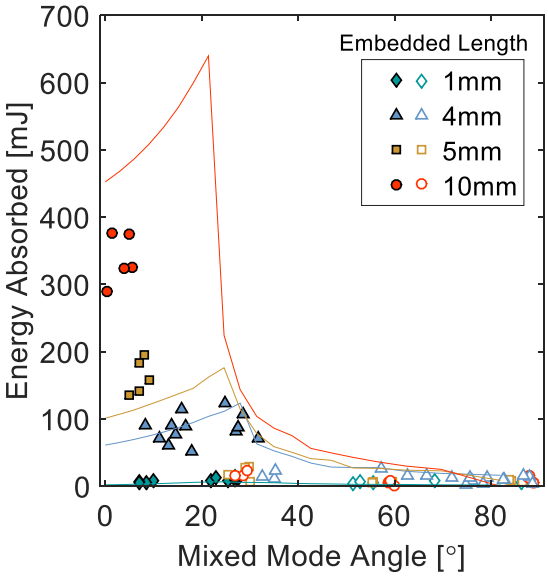

Figure 7 Original bridging traction model (solid lines) predicting the Z-pin energy absorption with increasing mixed mode angles

Although the original model is capable of demonstrating the trend of the bridging traction energy for increasing mixed mode angle, it does not fully capture the variation in pull-out energy absorbed and transition regions for increasing Z-pin embedded length. The lack of sensitivity of the transition region to increase in the embedded length is due to the definition of the failure criterion which assumes any transverse stress contribution to the Z-pin can be captured in the bending moment along the pin axis, only. The under prediction of the pull-out energy for the 1mm and 5mm and over prediction for the 10mm embedded lengths is due to the definition of the tangential friction forces. For this reason, the tangential friction forces exerted at the Z-pin/resin interface need to be considered in greater detail.

5.1 Non-linear tangential friction force

The two stage pull-out response of the Z-pin has been defined as the initial elastic rise before pin/matrix dis-bond followed by pin pull-out from the laminate [4,7,9]. The pin/matrix bond strength contribution to the traction loads is shown to be very small. This is due to the lateral thermal contraction mis-match between the laminate and the Z-pin in multidirectional laminates, which generates residual stresses on the pin/matrix boundary, weakening the interface [4,13].

An observation on experimental results produced here and in [4,30] is the non-linear rise in traction load, reaching a maximum, after which the pull-out progresses with a decrease in the traction load due to the shortening of the remaining embedded length of the Z-pin. The nonlinear rise and fall of the traction load curve can be captured with a non-linear residual tangential frictional force per unit length of the Z-pin, p_{nl}. Allegri *et. al.* [24] used a three parameter exponential equation to represent this non-linear behaviour, which was independent from the embedded length.

Assuming for Mode I tests $U<<W$ then the remaining embedded length of the pin is αL-W. Thus p_{nl} can be defined as:

$$p_{nl} = \frac{P}{\alpha L - W} \tag{11}$$

Relative to opening displacement, W it can be observed that there exists a strong relationship between the embedded length and the non-linear force per unit length, p_{nl} as shown in Figure 8a. This phenomenon implies that some extra mechanisms contribute to the variable tangential friction load, that is strongly dependent on the embedded length of the Z-pin. This pull-out behaviour has been seen in multidirectional FRP composites [4,30] as well as neat resin [6], but not in UD composites [4,6] therefore the variable thermal contraction of the surrounding material along the Z-pin surface may be a contributing factor. This phenomenon will be explored in detail through micro-mechanical models in future work. The tangential friction load can be calculated by multiplying the non-linear tangential friction force per unit length, p_{nl} by the embedded length (αL) as is shown in Figure 8b. This shows that there exists a relationship between the tangential friction load and opening displacement, which can be defined by a power law empirical fit:

$$p_{nl}\alpha L = \lambda W^{1/2} \tag{12}$$

Where λ is a scaling constant, which is evaluated using a least square fit. By combining all three embedded lengths, λ is evaluated to be 1069 shown as the solid black lines in Figure 8. The power law curve with λ of 700 and 1300 highlight the approximate bounds of the large scatter in the experimental data in Figure 8b.

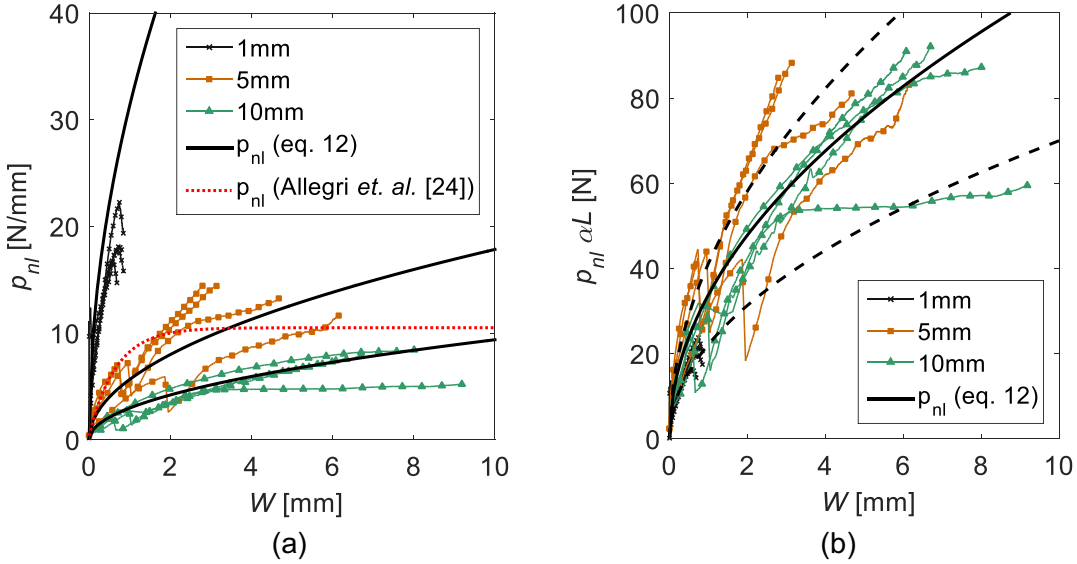

Figure 8 Mode I opening displacement against (a) tangential friction force (Solid line is empirical fit for λ=1069, dashed lines show approximate boundary to the data, with λ=700 and 1300) (b) tangential friction force per unit length (Solid line is empirical fit for λ=1069, dotted line is the original formulation from Allegri *et. al.* [24])

5.2 Modified bridging traction model

The Z-pin shown in Figure 6 is modelled as a Euler-Bernoulli beam subjected to a small but finite rotation. The equilibrium equations for an infinitesimal segment of the Z-pin were derived in [24] in the following form:

$$EI\frac{d^4u}{dz^4} - N\frac{d^2u}{dz^2} + \mathrm{q} = 0 \tag{13}$$

$$\frac{dN}{dz} = -EI\frac{d^3u}{dz^3}\frac{d^2u}{dz^2} - \mathrm{p} \tag{14}$$

Where u is the transverse displacement, N is the resultant axial force on the Z-pin cross-section, E is the Z-pin longitudinal modulus and I is the Z-pin cross-sectional second moment of area. The parameters p and q are distributed loads per unit length acting in the tangential and normal directions on the Z-pin lateral surface respectively. Three different distributed forces are considered to be acting on the Z-pin. These are the Winkler's foundation forces, residual frictional forces and Coulomb frictional forces [24]. Forces generated by Winkler's foundation have a magnitude that is proportional to the relative displacement between the Z-pin and the surrounding laminate and opposite in direction, thus for the normal direction this is:

$$q = \begin{cases} k_x u, & 0 \le z \le \alpha L - W \\ k_x(u - U), & \alpha L \le z \le L \end{cases} \tag{15}$$

Where k_x is the foundation stiffness of the sub-laminates. In a mixed-mode regime, the Coulomb friction associated with the transverse foundation forces in Eq. (15) will increase the distributed tangential load [28]. The tangential frictional forces acting on a Z-pin can be written as:

$$p = \begin{cases} -p_{nl} - \mu k_x|u|, & 0 \le z \le \alpha L - W \\ p_{nl} + \mu k_x|u - U|, & \alpha L \le z \le L \end{cases} \tag{16}$$

Where μ is the coefficient of coulomb friction, and p_{nl} is the non-linear residual frictional force per unit length defined in equation (12).

The following normalised variables for the total displacement, δ, opening displacement, W, the relative transverse displacement, U, transverse displacement along the Z-pin axis, u, the axial abscissa, z and the resultant axial force on the Z-pin cross section, N are defined:

$$d = \frac{\delta}{L^-} \qquad w = \frac{W}{L^-} \qquad Y = \frac{U}{D} \qquad y = \frac{u}{D} \qquad \xi = \frac{z}{L} \qquad n = \frac{NL^2}{EI} \tag{17}$$

Using equations (14-16), with the normalised variables from equation (17), the governing relationships for the normalised transverse displacement and axial force can be defined using a set of non-linear ordinary differential equations for each segment of the Z-pin:

$$\frac{d^4y}{d\xi^4} - n\frac{d^2y}{d\xi^2} = y^{iv} - ny'' = \begin{cases} -\dfrac{L^4}{EI}k_x y, & 0 \le \xi \le \alpha(1-d) \\ 0, & \alpha(1-d) < \xi < \alpha \\ -\dfrac{L^4}{EI}k_x(y - Y), & \alpha < \xi < 1 \end{cases} \tag{18a}$$

$$\frac{dn}{d\xi} = n' = \begin{cases} -\left(\dfrac{D}{L}\right)^2 y'''y'' + \dfrac{L^3}{EI}(p_{nl} + D\mu k_x|y|), & 0 \le \xi \le \alpha(1-d) \\ 0, & \alpha(1-d) < \xi < \alpha \\ -\left(\dfrac{D}{L}\right)^2 y'''y'' - \dfrac{L^3}{EI}(p_{nl} + D\mu k_x|y - Y|), & \alpha < \xi < 1 \end{cases} \tag{15b}$$

and by virtue of equation (10) and (17) Y is given by

$$Y = \frac{\phi\alpha L d}{D} \tag{19}$$

Note that assuming that the Z-pins are moderately slender, i.e.

$$\left(\frac{D}{L}\right)^2 \ll 1 \tag{20}$$

The first terms on the right hand side of equation (14b) can be removed.

Continuity conditions are imposed for the normalised transverse displacement, rotation, bending moment, shear force and axial force at the location joining the lower embedded segment, the pulled out portion and the upper embedded segment.

The model defined in equation (14) is implemented in MATLAB using the non-linear boundary value problem solver, BVP4C along with the boundary conditions defined in [24] as follows:

$$y(0) = 0 \qquad y(1) = Y \qquad \frac{dy(1)}{d\xi} = 0 \qquad \frac{dn(0)}{d\xi} = 0 \qquad \frac{d^2y(0)}{d\xi^2} = 0 \tag{21}$$

For any input of mixed mode ratio, ϕ and normalised displacement, d the solution of equation (14) will yield the normalised transverse displacement and forces along the axis of the Z-pin. For moderately slender Z-pins stated in (20), the pin cross-sectional resultant forces projected on the z and x axes [24] are:

$$\bar{Z} = \frac{EI}{L^2}n$$
$$\bar{X} = \frac{EID}{L^3}(ny' - y''') \tag{22}$$

Where $\bar{Z}$ and $\bar{X}$ are the axial and shear bridging forces on the z and x axes respectively. For each analysis, normalised total displacement, d is incremented between 0 and 1 and forces along the Z-pin axis are evaluated until the pin has fully pulled-out (d=1) or linear failure criterion limit in equation (7) has been reached.

For each mixed mode ratio and normalised opening displacement, the total bridging traction load was measured at the mid-section of the Z-pin. Once the P-δ curves have been obtained, the total Z-pin traction energy absorbed, Ω can be calculated as before, using equation (6). Using a foundation stiffness k_x of 700N/mm^2 (see section 5.3.2) and λ of 1069 the modified Z-pin bridging traction model is calculated for 100 discretised points over mixed mode ratios between 0 and 1. The material properties and parameters are given in Table 1. Validation of the modified bridging model is carried

out against the 10mm embedded length samples tested at mixed mode angles ranging from ω=3° to ω=82° as shown in Figure 9.

Table 1 Material properties and parameters used for the modified Z-pin bridging traction model

Z-Pin Material Property			Z-Pin Interface Friction properties		
$\boldsymbol{E}$	133GPa	[29]	$\boldsymbol{\lambda}$	1069	
$\boldsymbol{\sigma_{zf}}$	2026MPa	[29]	$\boldsymbol{\mu}$	0.7	[31]
$\boldsymbol{\tau_{xf}}$	485MPa		$\boldsymbol{k_x}$	700N/mm^2	

Very good agreement between the model prediction and the test results were obtained. The model predicts the full pull-out curve correctly and the specimens on the transition between pull-out and fracture are also captured well.

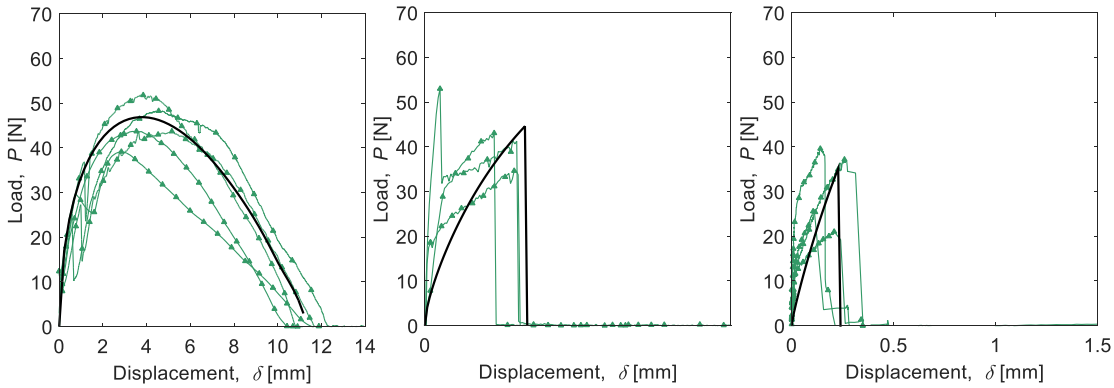

Figure 9 Validation of load–displacement model predictions (solid black lines) against experimental curves (green lines with symbol) of embedded length, $\bar{L}$=10mm

The total Z-pin traction energy absorbed, Ω against mixed mode angle for embedded lengths, 1mm, 5mm and 10mm are plotted against the experimental data investigated here and 4mm embedded length investigated previously by Yasaee *et. al.* [4] in Figure 10. Compared with the predictions of the original model in Figure 7, the modified formulation gives good agreement in the energy absorption in the pull-out region for the three embedded lengths tested here. The new formulation captures a distinct receding angle where pull-out/failure transition occurs with increasing in embedded length.

For the experimental data of the previous study on 4mm embedded length, the calculation of the pull-out bridging energies is over predicted and the mode II bridging energies is under predicted. This highlights the variability of the Z-pin material batches used for each study. The Z-pin/Matrix interface friction property of the Z-pin materials used here is higher whereas the effective shear strength is

lower. This underlines the challenges involved with testing and modelling of Z-pinned composites where batch to batch variability of the materials may vary significantly over time.

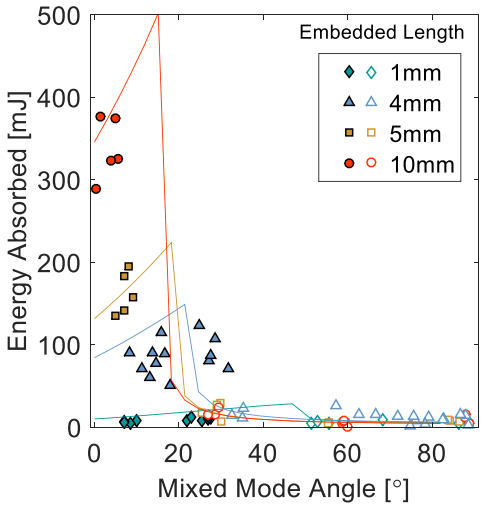

Figure 10 Modified bridging traction model (solid lines) predicting the Z-pin energy absorption with increasing mixed mode angles for increasing embedded lengths

The modifications to the model presented here requires only two parameters to be calibrated k_x and λ as opposed to six in the original formulation. Both these parameters can be determined using mode I and mode II single pin experimental tests for a single embedded length only. This significantly reduces the experimental data required for model calibration and validation if new Z-pin material batches are to be used. Further behaviour of the model characteristics and their influence on the bridging energy response is discussed in more detail in the following section.

5.3 Characteristics of the model

5.3.1 Tangential friction force

The tangential friction force for the Z-pin material and geometry presented here was modelled with the power law relationship given in equation (12). The scaling constant λ of 1069 was fitted to the average of the experimental data, however the large scatter in the experimental data are highlighted by the approximate bounds power law curve with λ of 700 and 1300. The influence of the scaling constant on the bridging traction model response for embedded lengths 5 and 10mm is shown in Figure 11. An increase in λ implies a higher tangential friction force and thus causes an increase in pull-out energy.

The increase in pull-out energy however is accompanied by a shift toward mode I of the transition region due to the high forces leading to fracture at lower mixed mode ratios.

These results clearly show that although increasing friction may benefit the mode I dominated bridging traction response, the shift in transition region implies reduced performance for large portions of the mixed mode I/II energy curve.

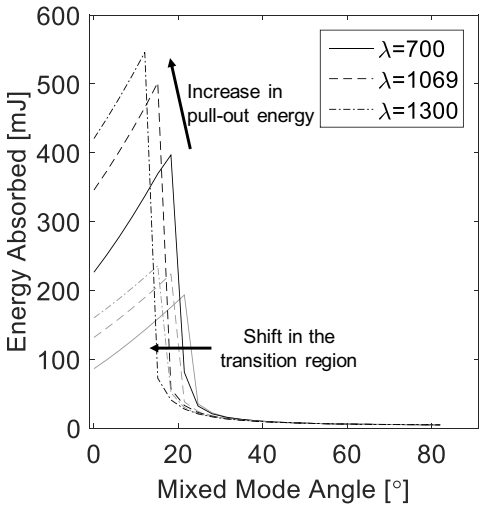

Figure 11 Influence of increasing λ on the pull-out energy and transition region (Embedded length, L^{-}=5mm (light) and 10mm (dark))

5.3.2 Foundation stiffness

The foundation stiffness, k_x, is equivalent to the local elastic stiffness of the embedding laminate. Given that it is not possible to directly measure this value from the current experimental data; the foundation stiffness was calibrated against the traction response of the mode II loading tests. The mode II loads for the 10mm embedded length sample batch are given in Figure 12a with the analytical model predictions using k_x values ranging from 0 to 1000N/mm^2. Setting the foundation stiffness to zero produces a very low traction stiffness with failure displacement far greater than 1mm. Increasing the foundation stiffness to 200N/mm^2 significantly increases the traction stiffness response with predicted failure displacement of 0.66mm. Foundation stiffness of 500 to 1000N/mm^2 produces failure displacements within the experimental scatter. The influence of the k_x on the bridging energy is shown in Figure 12b. With increasing k_x from 50N/mm^2, the energy absorbed in the mode II dominated regions becomes lower and the transition region shifts towards mode I. For pure mode I pull-out

(Φ=0), the foundation stiffness has no influence on the pull-out energy. As the mode II component of the load increases the energy absorbed (in the pull-out regime) increases. An increasing foundation stiffness causes an increase in the slope of this curve.

The foundation stiffness defined here is analogous to punch strength defined by Cox [28] and Plain and Tong [31], who argued that the punch strength is equivalent to 2.83 times the material's compression strength and may vary between 300 to 1000N/mm^2 depending on the laminate layup. The transverse compression strength of a UD IM7/8552 material is 199.8MPa [32], which would correspond to a 565N/mm^2 foundation stiffness and for a QI laminate it is 657MPa [33], corresponding to 1859N/mm^2 foundation stiffness. Given that the majority of the punching force experienced near the fracture plane is expected to be between 565 and 1859N/mm^2, the calibrated value to be 700N/mm^2 is considered to be reasonable. Whilst foundation stiffness is an important parameter for the bridging traction behaviour, the foundation stiffness will vary only by a small amount for most multidirectional polymeric fibre composites.

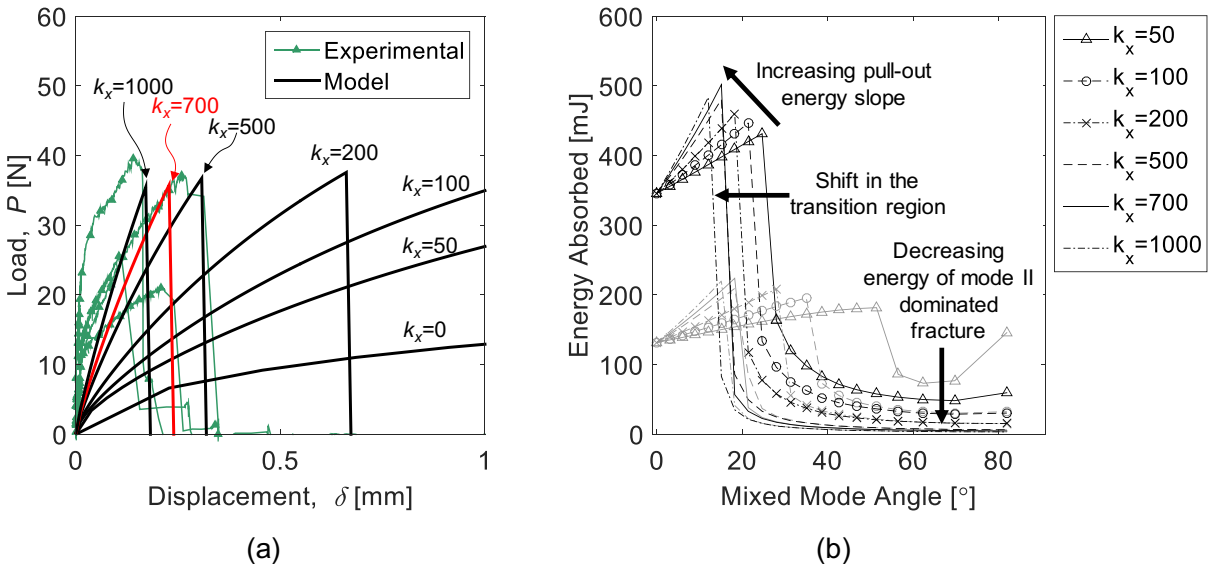

Figure 12 Influence of the foundation stiffness, k_x (units N/mm^2) for the prediction of (a) traction load response of Z-pins loaded in the mode II dominated (ϕ = 0.99) regime, (Embedded length, L^-=10mm) (b) Z-pin energy absorption with increasing mixed mode angles (Embedded length, L^-=5mm (light) and 10mm (dark))

5.3.3 Pin Failure strength

The influence of pin failure strength on the bridging traction model response for embedded lengths 5 and 10mm is shown in Figure 13. Fixing the tensile failure strength at 2026MPa and reducing the

effective shear strength of the Z-pin, the transition region is shown to reduce monotonically in Figure 13a. As expected, the mode II dominated failure energy does see a significant reduction with reduced effective shear strength, but its absolute magnitude is small compared to the Mode I dominated end of the curve. Fixing the effective shear strength of the Z-pin at 485MPa and reducing the tensile strength, sees a shift in the transition region towards lower mixed mode angle as shown in Figure 13b. Tensile strength has little influence on the mode II dominated bridging energy. These results indicate that higher strength in both transverse and tensile direction is desired to increase the bridging energy absorption across all mixed mode rations for improved performance.

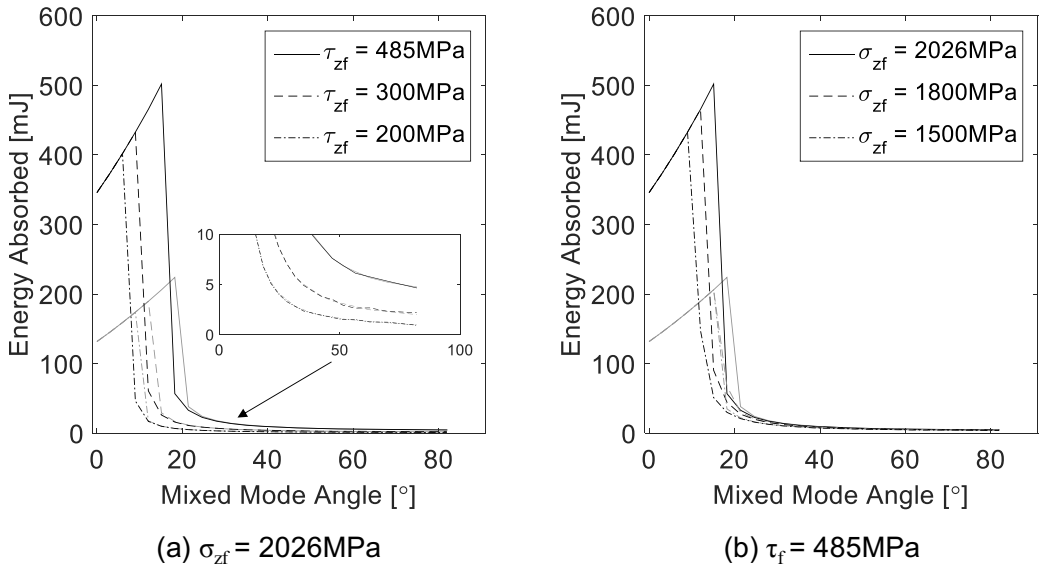

Figure 13 Z-pin energy absorption with increasing mixed mode angles predicted with (a) decreasing effective shear strength for fixed tensile strength of 2026MPa (b) Decreasing tensile strength for fixed effective shear strength of 485MPa (Embedded length, L^{-}=5mm (light) and 10mm (dark))

6 Conclusions

An experimental characterisation of the influence of Z-pin embedded length on the traction response of multidirectional FRP composite has been presented across the full mode mixity range. The experimental data revealed a non-linear relationship between the tangential friction load per unit length of the Z-pin against pull-out displacement. This relationship was also shown to be strongly influenced by the embedded length of the Z-pin. A new power law empirical relationship was proposed to characterise the non-linear friction response. This new relationship was used to modify an

analytical model developed by Allegri *et. al.* [24] along with an updated failure criterion definition. This model showed very good agreement with experimental tests carried out in this investigation, in particular for predicting the pull-out regime bridging traction response. Several characteristics of the model were discussed and their influence on the predicting the Z-pin bridging energy response were analysed.

Although this model does not have sufficient fidelity to fully explain all of the physical behaviour of Z-pin failure (e.g. internal splitting), with the measured homogenised effective shear strength of the Z-pin, it is capable of predicting the trend of a full mixed mode bridging mechanics of a 0.28mm CFRP pin with varying embedded lengths in a multidirectional composite laminate with a very good level of accuracy.

7 References

[1] Mouritz AP. "Review of z-pinned composite laminates," *Composites Part A: Applied Science and Manufacturing*, vol. 38, no. 12, pp. 2383–2397, 2007.

[2] Partridge IK, Yasaee M, Allegri G, Lander JK. "Damage-tolerant composite structures by Z-pinning," in *Toughening Mechanisms in Composite Materials*, Elsevier, 2015, pp. 161–189.

[3] Sam Huang H, Waas AM. "Quasi-static mode II fracture tests and simulations of Z-pinned woven composites," *Engineering Fracture Mechanics*, vol. 126, pp. 155–165, 2014.

[4] Yasaee M, Lander J, Allegri G, Hallett S. "Experimental characterisation of mixed mode traction–displacement relationships for a single carbon composite Z-pin," *Composites Science and Technology*, vol. 94, pp. 123–131, 2014.

[5] Toral Vazquez J, Castanié B, Barrau JJ, Swiergiel N. "Multi-level analysis of low-cost Z-pinned composite joints: Part 1: Single Z-pin behaviour," *Composites Part A: Applied Science and Manufacturing*, vol. 42, no. 12, pp. 2070–2081, Dec. 2011.

[6] Cartié DDR, Cox BN, Fleck NA. "Mechanisms of crack bridging by composite and metallic rods," *Composites Part A: Applied Science and Manufacturing*, vol. 35, no. 11, pp. 1325–1336, Nov. 2004.

[7] Mouritz AP, Koh TM. "Re-evaluation of mode I bridging traction modelling for z-pinned laminates based on experimental analysis," *Composites Part B*, vol. 56, pp. 797–807, 2014.

[8] Cui H, Li Y, Koussios S, Beukers A. "Mixed mode cohesive law for Z-pinned composite analyses," *Computational Materials Science*, vol. 75, pp. 60–68, Jul. 2013.

[9] Cui H, Li Y, Koussios S, Zu L, Beukers A. "Bridging micromechanisms of Z-pin in mixed mode delamination," *Composite Structures*, vol. 93, no. 11, pp. 2685–2695, Oct. 2011.

[10] Mohamed G, Helenon F, Allegri G, Yasaee M, Hallett SR. "Predicting the through-thickness enhancement of z-pinned composite laminates," in *19th International Conference on Composite Materials*, Montreal, Canada, 2013.

[11] Wang X, Chen L, Jiao Y, Li J. "Preparation of carbon fiber powder-coated Z-pins and experimental study on the mode I delamination toughening properties," *Polymer Composites*, p. n/a-n/a, May 2015.

[12] Dai S-C, Yan W, Liu H-Y, Mai Y-W. "Experimental study on z-pin bridging law by pullout test," *Composites Science and Technology*, vol. 64, no. 16, pp. 2451–2457, 2004.

[13] Sweeting RD, Thomson RS. "The effect of thermal mismatch on Z-pinned laminated

composite structures," *Composite structures*, vol. 66, pp. 189–195, 2004.
[14] Pegorin F, Pingkarawat K, Daynes S, Mouritz AP. "Mode II interlaminar fatigue properties of z-pinned carbon fibre reinforced epoxy composites," *Composites Part A: Applied Science and Manufacturing*, Aug. 2014.
[15] Yasaee M, Mohamed G, Hallett SR. "Multiple delamination interaction in Z-pinned composites in Mode II," *Experimental Mechanics*, 2016.
[16] Pegorin F, Pingkarawat K, Daynes S, Mouritz AP. "Influence of z-pin length on the delamination fracture toughness and fatigue resistance of pinned composites," *Composites Part B: Engineering*, vol. 78, pp. 298–307, Sep. 2015.
[17] Cox B, Sridhar N. "A traction law for inclined fiber tows bridging mixed-mode cracks," *Mechanics of Advanced Materials and Structures*, no. 9, pp. 299–331, 2002.
[18] Grassi M, Zhang X. "Finite element analyses of mode I interlaminar delamination in z-fibre reinforced composite laminates," *Composites Science and Technology*, vol. 63, no. 12, pp. 1815–1832, Sep. 2003.
[19] Yan W, Liu H-Y, Mai Y-W. "Numerical study on the mode I delamination toughness of z-pinned laminates," *Composites Science and Technology*, vol. 63, no. 10, pp. 1481–1493, Aug. 2003.
[20] Allegri G, Zhang X. "On the delamination and debond suppression in structural joints by Z-fibre pinning," *Composites Part A: Applied Science and Manufacturing*, vol. 38, no. 4, pp. 1107–1115, Apr. 2007.
[21] Bianchi F, Zhang X. "A cohesive zone model for predicting delamination suppression in z-pinned laminates," *Composites Science and Technology*, vol. 71, no. 16, pp. 1898–1907, Nov. 2011.
[22] Bianchi F, Koh TM, Zhang X, Partridge IK, Mouritz AP. "Finite element modelling of z-pinned composite T-joints," *Composites Science and Technology*, vol. 73, pp. 48–56, Nov. 2012.
[23] Bianchi F, Zhang X. "Predicting mode-II delamination suppression in z-pinned laminates," *Composites Science and Technology*, vol. 72, no. 8, pp. 924–932, May 2012.
[24] Allegri G, Yasaee M, Partridge IK, Hallett SR. "A novel model of delamination bridging via Z-pins in composite laminates," *International Journal of Solids and Structures*, vol. 51, no. 19–20, pp. 3314–3332, Oct. 2014.
[25] Mohamed G, Yasaee M, Allegri G, Hallett SR. "Cohesive element formulation for Z-pin delamination bridging in fibre reinforced laminates," *International Journal of Solids and Structures (Submitted 21/03/2016)*.
[26] Toral Vazquez J, Castanié B, Barrau JJ, Swiergiel N. "Multi-level analysis of low-cost Z-pinned composite joints: Part 2: Joint behaviour," *Composites Part A: Applied Science and Manufacturing*, vol. 42, no. 12, pp. 2082–2092, Dec. 2011.
[27] Zhang B, Yasaee M, Hallett SR, Allegri G. "Micro-Mechanical Finite Element Analysis of Z-pins under Mixed-Mode Loading," *Composites Part A: Applied Science and Manufacturing*, 2015.
[28] Cox BN. "Snubbing Effects in the Pullout of a Fibrous Rod from a Laminate," *Mechanics of Advanced Materials and Structures*, vol. 12, no. 2, pp. 85–98, Mar. 2005.
[29] Zhang B, Allegri G, Yasaee M, Hallett SR, Partridge IK. "On the Delamination Self-Sensing Function of Z-pinned Composite Laminates," *Composite Science and Technology*, vol. 128, pp. 138–146, 2016.
[30] Zhang B, Allegri G, Yasaee M, Hallett SR, Partridge IK. "On the Delamination Self-Sensing Function of Z-pinned Composite Laminates," *Composite Science and Technology*, 2016.
[31] Plain KP, Tong L. "Traction law for inclined through-thickness reinforcement using a geometrical approach," *Composite Structures*, vol. 88, no. 4, pp. 558–569, May 2009.
[32] Camanho PP, Maimí P, Dávila CG. "Prediction of size effects in notched laminates using continuum damage mechanics," *Composites Science and Technology*, vol. 67, no. 13, pp. 2715–2727, 2007.
[33] Lee J, Soutis C. "A study on the compressive strength of thick carbon fibre–epoxy laminates," *Composites Science and Technology*, vol. 67, no. 10, pp. 2015–2026, 2007.

2016-11-10

Influence of Z-pin embedded length on the interlaminar traction response of multi-directional composite laminates

Yasaee, Mehdi

Elsevier

Yasaee M, Bigg L, Mohamed G, Hallett SR, Influence of Z-pin embedded length on the interlaminar traction response of multi-directional composite laminates, Materials & Design, þÿ V o l u m e 1 1 5 , 5 F e b r u a r y 2 0 1 7 , P a g e s 2 6 3 6
http://dx.doi.org/10.1016/j.matdes.2016.11.025